Mathematical and Computational Applications

MDPI

*Article*

# Traveling Waves, Bifurcation Analysis and Benjamin–Feir Instability in Schrödinger–Hirota Model with Power-Law of Self-Phase Modulation

**Oswaldo González-Gaxiola [1], Milisha Hart-Simmons [2], Ahmed H. Arnous [3,4] and Anjan Biswas [2,5,6,7,8,*]**

1 Applied Mathematics and Systems Department, Universidad Autónoma Metropolitana–Cuajimalpa, Vasco de Quiroga 4871, Mexico City 05348, Mexico; ogonzalez@cua.uam.mx
2 Department of Mathematics and Physics, Grambling State University, Grambling, LA 71245-2715, USA; simmonsmil@gram.edu
3 Department of Engineering Mathematics and Physics, Higher Institute of Engineering, El Shorouk Academy, El-Shorouk City 11837, Egypt; ahmed.h.arnous@gmail.com
4 Jadara Research Center, Jadara University, Irbid 21110, Jordan
5 Department of Mathematics, Faculty of Science, Karadeniz Technical University, Trabzon 61080, Türkiye
6 Department of Physics and Electronics, Khazar University, Baku AZ1096, Azerbaijan
7 Applied Science Research Center, Applied Science Private University, Amman 11937, Jordan
8 Department of Mathematics and Applied Mathematics, Sefako Makgatho Health Sciences University, Medunsa, Pretoria 0204, South Africa
* Correspondence: biswas.anjan@gmail.com

**Abstract**

We critically reexamine traveling-wave solutions and Benjamin–Feir instability for a Schrödinger–Hirota equation with power-law nonlinearity. A traveling-wave reduction, Hamiltonian phase-plane analysis, direct substitution, and symbolic residual checks are used to establish the compatibility of candidate solutions with the original complex equation. The previously reported unrestricted extended-Kudryashov solution family is shown to be invalid; only a restricted singular branch survives on a half-line and cannot represent a globally regular optical soliton. A regular bright solitary pulse is verified, and sign-changing dark waves are characterized through an implicit real quadrature rather than ambiguous fractional powers. The corrected Jacobian determinants yield consistent classifications of equilibria and their homoclinic or heteroclinic trajectories. For continuous-wave backgrounds, the perturbation dispersion relation determines the instability band and the corrected maximum growth rate. Explicit parameter sets and reproducibility checks distinguish valid traveling waves from singular profiles and clarify that instability of the background does not establish instability of localized solitons.

**Keywords:** Schrödinger–Hirota equation; power-law nonlinearity; extended Kudryashov audit; heteroclinic waves; bifurcation; Benjamin–Feir instability

Check for updates

Academic Editors: Gianluigi Rozza, Oliver Schütze and Nicholas Fantuzzi

Received: 22 September 2026
Revised: 25 October 2026
Accepted: 3 November 2026
Published: 5 November 2026

**Copyright:** © 2026 by the authors. Licensee MDPI, Basel, Switzerland. This article is an open access article distributed under the terms and conditions of the Creative Commons Attribution (CC BY) license.

## 1. Introduction

Optical envelope equations balance dispersion and nonlinear phase accumulation, and higher-order terms become relevant when a cubic nonlinear Schrödinger approximation is insufficient [1–3]. The higher-order nonlinear Schrödinger framework and related Schrödinger–Hirota reductions have been studied under additional dispersive and derivative effects [4–6]. The model considered here includes group-velocity dispersion (GVD), third-order dispersion (TOD), a power-law self-phase-modulation (SPM) term, and two

derivative nonlinearities. The last two are treated as independent phenomenological coefficients: identifying either term with a specific microscopic Raman response requires a separate dimensional and material derivation [7–9].

Power-law solitary waves are not new in themselves; their quadrature and phase-plane descriptions are well established in the non-Kerr literature [10]. Recent related work has investigated fractional nonlinear Schrödinger bifurcations and wave construction in optical-fiber models [11,12], while a separate higher-order, stochastic generalized nonlinear Schrödinger model illustrates the breadth of dispersive optical-soliton research [13]. Those distinct models are cited for context, not as verification of the present deterministic equation. Likewise, exact-solution algorithms must be accompanied by substitution tests, not only formal coefficient matching [14,15]. We therefore reassess which structures of the generalized Schrödinger–Hirota model are *actual* classical solutions. In particular, a rational extended-Kudryashov ansatz can produce an isolated pole-type branch, but not the previously claimed unrestricted one-parameter family. The distinction between a smooth dark kink and a fractional power of a sign-changing auxiliary function is essential when $n$ is noninteger.

The specific contribution is a consistency-tested account combining (i) explicit compatibility conditions for both parts of the original complex partial differential equation (PDE), (ii) positive bright pulses and smooth sign-changing heteroclinic waves for continuous $n > 0$, together with the domain of an isolated singular Kudryashov branch, (iii) the corrected equilibrium determinant and boundary classification, and (iv) a rechecked Benjamin–Feir (modulation) instability (MI) dispersion relation and maximum growth rate. The exact bright profile and the classical cubic kink are not presented as newly discovered solution forms. The novelty claimed is limited to the joint consistency and parameter-level characterization for this particular higher-order model. Numerical graphics and explicit parameter-level substitution checks are presented in the article for reproducibility.

The physical motivation for this analysis is the competition between dispersion and nonlinear phase modulation in guided optical pulses. In the standard envelope approximation, group-velocity dispersion can counteract the intensity-dependent refractive-index response and support localized traveling pulses. For sufficiently short pulses, higher-order dispersion and intensity-gradient effects may alter the propagation dynamics, so the mathematical conditions supporting a wave need to be checked for the particular higher-order equation under study. These mechanisms motivate the normalized equation, but they do not by themselves identify the coefficients with experimentally measured properties of a particular optical material. This distinction is consistent with the broader nonlinear-fiber-optics literature [16].

An additional mathematical issue arises when the nonlinear response is described by a noninteger power of the intensity. The complex field nonlinearity is gauge invariant, but a real traveling-wave amplitude may take either sign. Consequently, replacing an absolute-value nonlinearity by an unrestricted algebraic power can invalidate a proposed profile at a zero crossing. Exact-solution constructions also require careful treatment of integration constants, boundary conditions at both spatial infinities, and possible poles. These requirements are particularly important for rational auxiliary-function schemes: solving an algebraic coefficient system is only an intermediate step, and a candidate profile must still satisfy the original partial differential equation on its claimed domain.

Prior work on generalized nonlinear Schrödinger models with nonlinear dispersion and arbitrary refractive-index laws provides a useful benchmark for stationary solitary-wave construction [17]. In a related, but different, optical setting, Zayed and coauthors investigated quiescent solitons in magneto-optic waveguides with Kudryashov-type self-phase modulation using algebraic and auxiliary-equation methods [18]. These studies

concern different equations and do not validate solutions of the present Schrödinger–Hirota model; instead, they motivate a precise comparison of constitutive assumptions, compatibility conditions, and direct residual checks.

The phase-plane and spectral viewpoints provide complementary, but logically different, information. Homoclinic and heteroclinic energy levels characterize the boundary behavior of solitary pulses and kink-type waves, as illustrated in a related higher-order nonlinear Schrödinger setting by Ouyang and coauthors [19]. By contrast, Benjamin–Feir or modulation instability concerns the response of a continuous-wave background to infinitesimal sidebands. A recent study of higher-order dispersion by Runge and coauthors emphasizes the sensitivity of modulation-instability dynamics to a dispersive structure [20]. Neither the existence of a phase-plane separatrix nor the instability of a uniform background by itself establishes the spectral stability of a localized solitary wave.

With these distinctions in place, the analysis below proceeds from the normalized field equation and its compatibility conditions to a direct audit of the rational ansatz. It then constructs regular and singular traveling-wave branches, relates their boundary conditions to Hamiltonian trajectories, and independently derives the continuous-wave instability spectrum. Throughout, the emphasis is on exact substitution, explicit parameter choices, and the limits of the conclusions, rather than on unsupported claims of a new unrestricted soliton family.

## 2. Power-Law Schrödinger–Hirota Model

We begin by specifying the higher-order envelope equation that will be analyzed. The purpose of this section is to separate the structure of the normalized mathematical model from a material-specific optical interpretation. In particular, the linear dispersive terms, the generalized self-phase-modulation response, and the derivative nonlinearities play different roles in a traveling-wave reduction. Their coefficients are taken as real model parameters; identifying them with experimentally measured self-steepening or delayed Raman constants would require additional constitutive assumptions and dimensional scaling, which are outside the scope of this work [7,16].

Consider

$$iq_t + aq_{xx} + b|q|^{2n}q + i\left[\alpha q_{xxx} + \beta|q|^{2n}q_x + \gamma\left(|q|^{2n}\right)_x q\right] = 0, \tag{1}$$

where $q(x,t)$ is complex, the coordinates are normalized, $a, b, \alpha, \beta, \gamma$ are real, and $n > 0$ (including the interval $0 < n < 2$ examined in the figures). Here, $a$ represents GVD, $\alpha$ TOD, $b$ SPM, and $\beta, \gamma$ independent derivative nonlinearities. The term containing $\beta$ changes the local intensity-dependent transport, whereas the $\gamma$ term acts through the spatial intensity gradient. No material-specific interpretation is asserted without a constitutive model. A continuous-wave (CW) background is a nonzero spatially uniform solution. The Benjamin–Feir criterion below tests *CW* stability and does not establish spectral stability of localized solitary waves.

## 3. Traveling-Wave Reduction and Compatibility

A traveling-wave profile obtained from a complex evolution equation is admissible only when the real and imaginary equations are satisfied simultaneously. This requirement is stronger than solving a single ordinary differential equation obtained after an algebraic simplification. We therefore first derive both amplitude equations, retain the absolute-value dependence required by a real signed envelope, and identify sufficient relations among the original coefficients that make the two reductions compatible. The ensuing residual identities supply a direct check of any bright, dark, or singular profile proposed later.

Let

$$q(x,t) = U(\xi)e^{i(kx-\omega t)}, \qquad \xi = x - vt, \qquad U(\xi) \in \mathbb{R}. \tag{2}$$

It is important to retain the absolute value of the real envelope. Taking real and imaginary parts of Equation (1) gives

$$(a - 3\alpha k)U'' + (\omega - ak^2 + \alpha k^3)U + (b - \beta k)|U|^{2n}U = 0. \tag{3}$$

$$\alpha U''' + (2ak - 3\alpha k^2 - v)U' + (\beta + 2n\gamma)|U|^{2n}U' = 0. \tag{4}$$

The derivative identity $\frac{d}{d\xi}(|U|^{2n}U) = (2n+1)|U|^{2n}U'$ is valid at $U = 0$ for $n > 0$. Nevertheless, the original $\gamma(|q|^{2n})_x q$ term contains the derivative of $|q|^{2n}$ *before* multiplication by $q$. At a simple zero of $U$ that derivative exists pointwise if $n > 1/2$. Accordingly, when $\gamma \neq 0$ the smooth sign-changing PDE profiles below are asserted as global classical solutions for $n > 1/2$; for $0 < n \leq 1/2$ the signed amplitude ODE remains meaningful but the unreduced PDE needs a weak/product-extension interpretation at the zero. (The bright profile is nonzero at every finite $\xi$.) Integrating the imaginary equation yields

$$\alpha U'' + (2ak - 3\alpha k^2 - v)U + \frac{\beta + 2n\gamma}{2n+1}|U|^{2n}U = C. \tag{5}$$

The integration constant $C$ is zero for a bright pulse with $U, U', U'' \to 0$ at both infinities. It is also zero for the symmetric kink considered below because its two asymptotic states $\pm U_*$ have opposite signs and the remaining coefficients are odd functions of $U$. A nonzero constant or asymmetric plateau requires separate analysis and is not considered here.

Set $D = a - 3\alpha k \neq 0$ and assume $\alpha \neq 0$. The two real equations are compatible with a common amplitude equation if

$$\frac{\omega - ak^2 + \alpha k^3}{D} = \frac{2ak - 3\alpha k^2 - v}{\alpha} = c_1, \qquad \frac{b - \beta k}{D} = \frac{\beta + 2n\gamma}{(2n+1)\alpha} = c_2. \tag{6}$$

Consequently the *signed* real amplitude solves

$$U'' + c_1 U + c_2|U|^{2n}U = 0. \tag{7}$$

To verify a proposed profile against the *original PDE*, denote the left side of (7) by $F[U]$. After substitution into (3) and (4) the respective residuals reduce exactly to

$$R_{\text{real}} = DF[U], \qquad R_{\text{imag}} = \alpha\frac{dF[U]}{d\xi}. \tag{8}$$

Thus a $C^3$ solution of (7) with (6) satisfies *both* equations, rather than only a partially reduced ODE. These identities also prescribe a transparent numerical residual check.

## 4. Auditing the Extended Kudryashov Ansatz

The extended Kudryashov approach replaces a differential equation by polynomial conditions for the coefficients of a rational auxiliary-function ansatz. Its appeal is computational: the Riccati auxiliary equation allows derivatives of the ansatz to be expressed algebraically in the auxiliary variable. However, a formally consistent balance of polynomial degrees does not imply that a reported solution of the coefficient conditions is correct. This section tests the earlier unrestricted family by exact substitution, examines its asymptotic and singularity structure, and determines whether any restricted branch survives. The audit also distinguishes a local singular solution from a globally regular optical soliton [14,15].

On an interval where $U > 0$, the transformation $V = U^n$ gives

$$nVV'' + (1-n)(V')^2 + c_1 n^2 V^2 + c_2 n^2 V^4 = 0. \tag{9}$$

This polynomial form is *not* a license to raise negative real bases to arbitrary fractional powers. For the Riccati function

$$Q' = Q^2 - Q, \qquad Q(\xi) = \frac{1}{1+e^{\xi}}, \qquad 0 < Q < 1, \tag{10}$$

consider the rational extension

$$V(Q) = \frac{a_0 + a_1 Q + a_2 Q^2}{1 + b_1 Q}. \tag{11}$$

Writing $\mathcal{D} = (Q^2 - Q)\partial_Q$, the nine coefficient constraints can be computed *without transcription* as the coefficients of $Q^0, \ldots, Q^8$ in

$$\mathcal{P}(Q) = (1 + b_1 Q)^4 \big[ nV\mathcal{D}^2 V + (1-n)(\mathcal{D}V)^2 + c_1 n^2 V^2 + c_2 n^2 V^4 \big]. \tag{12}$$

Candidate profiles obtained from these constraints are subsequently checked by direct substitution into the amplitude equation.

The formerly proposed family,

$$V_{\text{old}}(\xi) = \frac{A[(2-b_1)e^{\xi} + (2+b_1)]}{2(e^{\xi}+1)(e^{\xi}+b_1+1)}, \quad A = \frac{1}{n}\sqrt{-\frac{n+1}{c_2}}, \quad c_1 = -\frac{1}{n^2}, \tag{13}$$

is *not* an exact free-$b_1$ solution. In fact, with $n = 1$, $c_1 = c_2 = -1$, $b_1 = 1$, and $\xi = 0$, direct evaluation gives

$$\big[VV'' - V^2 - V^4\big]_{\xi=0} = -\frac{7}{27} \neq 0. \tag{14}$$

In addition, $V_{\text{old}}(+\infty) = 0$ but $V_{\text{old}}(-\infty) = A(2+b_1)/[2(1+b_1)]$ for generic $b_1$. Hence, $a_0 = 0$ does not impose two-sided zero boundary conditions. If $b_1 < -1$, the denominator can vanish at a finite real coordinate. The old limiting construction of a dark soliton is withdrawn.

One *restricted* Kudryashov solution remains valid: for $b_1 = -2$, $a_0 = 0$, $a_1 = 2A$, $a_2 = -2A$,

$$V(\xi) = A\ \operatorname{csch}\xi, \quad c_1 = -\frac{1}{n^2}, \quad c_2 = -\frac{n+1}{n^2A^2}, \quad A > 0. \tag{15}$$

For $\xi > 0$ the associated *one-sided* real solution is

$$U(\xi) = [A \operatorname{csch}\xi]^{1/n}, \qquad \xi > 0. \tag{16}$$

Indeed, $U''/U = 1/n^2 + (n+1)\operatorname{csch}^2\xi/n^2$ and $U^{2n} = A^2\operatorname{csch}^2\xi$, so (7) vanishes identically. The pole at $\xi = 0$ means this is *not* a global classical optical soliton. Its sign-changing continuation by an unqualified $1/n$ power is not used. For $n = 1$, the usual real signed continuation exists on each half-line separately but remains singular at the pole.

## 5. Regular Bright and Dark Waves

Once the amplitude equation and its parameter compatibility conditions have been established, the principal traveling-wave regimes can be distinguished by their endpoint behavior. A bright pulse approaches the zero background at both ends and corresponds to a homoclinic energy level, whereas a sign-changing dark-amplitude wave approaches two nonzero equilibria and corresponds to a heteroclinic orbit. Singular formulas must be assigned a domain excluding their poles. The constructions below use these boundary conditions explicitly and do not infer a dark wave from an invalid limit of the discarded rational family.

### *5.1. Bright Pulse and Direct PDE Verification*

For the focusing-sign regime of the reduced amplitude equation, the zero-energy first integral gives a positive localized pulse. We present its standard hyperbolic-secant representation and verify it by differentiation, then provide a complete set of original model parameters so that the result is not merely a formal solution of the reduced equation. The explicit solution is used as a benchmark for the compatibility and residual tests, not claimed as a newly discovered functional form.

For $c_1 = -\lambda^2 < 0$, $c_2 > 0$, the positive homoclinic profile is

$$U_{\mathrm{b}}(\xi) = \left(\frac{(n+1)\lambda^2}{c_2}\right)^{1/(2n)} \operatorname{sech}^{1/n}(n\lambda\xi), \qquad \lambda > 0. \tag{17}$$

It is smooth for every $n > 0$ and tends to zero on both sides. Direct differentiation yields

$$\frac{U_{\mathrm{b}}''}{U_{\mathrm{b}}} = \lambda^2 - (n+1)\lambda^2 \operatorname{sech}^2(n\lambda\xi), \quad c_2 U_{\mathrm{b}}^{2n} = (n+1)\lambda^2 \operatorname{sech}^2(n\lambda\xi). \tag{18}$$

Consequently $F[U_{\mathrm{b}}] \equiv 0$; its derivative also vanishes, so both complex PDE residuals in (8) are exactly zero. This is a standard quadrature-derived solution, not a free-parameter Kudryashov discovery.

For an explicit consistent fractional-power case choose

$$(n, a, b, \alpha, \beta, \gamma, k, \omega, v) = (0.8, 4, 2, 1, 1, 1, 1, 2, 6). \tag{19}$$

These values give $D = 1$, $(c_1, c_2) = (-1, 1)$ and $\lambda = 1$. Figure 1 displays the exact intensity $|q|^2 = U_{\mathrm{b}}^2$.

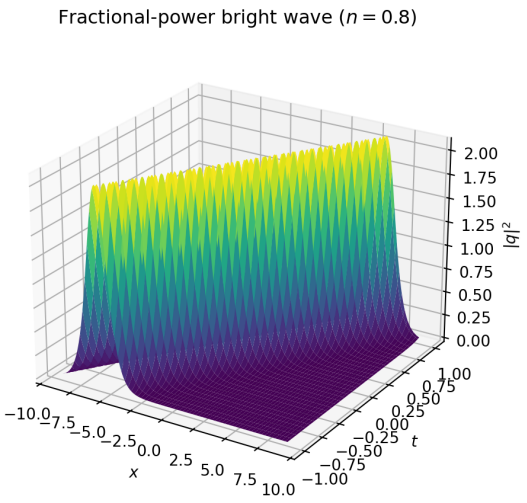



**Figure 1.** Bright-wave intensity $|q(x,t)|^2$ for $(n, a, b, \alpha, \beta, \gamma, k, \omega, v) = (0.8, 4, 2, 1, 1, 1, 1, 2, 6)$.

### *5.2. Fractional-Power Heteroclinic Wave*

The nonzero-background regime requires a different construction. For a general noninteger power, an arbitrary fractional power of a sign-changing hyperbolic tangent does not define a globally real smooth amplitude. We instead characterize the kink by a real energy quadrature connecting two symmetric equilibria. This makes the sign change, the boundary conditions, and the regularity restriction at the zero explicit; the elementary cubic kink is recovered only as a special case.

For $c_1 > 0, c_2 < 0$, define

$$U_* = \left(-\frac{c_1}{c_2}\right)^{1/(2n)}, \qquad H_* = \frac{n c_1 U_*^2}{2(n+1)}. \tag{20}$$

The monotone heteroclinic solution is defined by the real quadrature

$$\xi - \xi_0 = \int_0^{U(\xi)} \frac{ds}{\sqrt{2H_* - c_1 s^2 - \frac{c_2}{n+1}|s|^{2n+2}}}, \qquad -U_* < U(\xi) < U_*. \tag{21}$$

The square root is strictly positive inside this interval and vanishes linearly in $|U \mp U_*|$ at its endpoints, giving infinite tails. Therefore, $U(-\infty) = -U_*$, $U(+\infty) = U_*$, and $U'(0) = \sqrt{2H_*} > 0$ if $\xi_0 = 0$. The autonomous equation has a continuously differentiable force for every $n > 0$, so the signed amplitude $U$ is $C^3$ at its zero. When $\gamma \neq 0$, it also gives a classical pointwise solution of the original PDE across that zero for $n > 1/2$; the lower-exponent qualification in Section 3 applies. In contrast, a fractional power of $\tanh \xi$ is generally not a real differentiable function across the sign change.

The elementary cubic $(n = 1)$ special case is

$$U_{\mathrm{d}}(\xi) = U_* \tanh\left(\sqrt{c_1/2}\,\xi\right), \qquad n = 1, \tag{22}$$

which satisfies (7) for $c_1 > 0, c_2 < 0$. It is *not* obtained by taking a limit of (13). The cubic example $(n, a, b, \alpha, \beta, \gamma, k, \omega, v) = (1, 4, -6, 1, -5, 1, 1, 4, 4)$ yields $(c_1, c_2) = (1, -1)$ and validates both original PDE components by (8).

For fractional $n = 0.8$, the independent consistent PDE choice

$$(n, a, b, \alpha, \beta, \gamma, k, \omega, v) = (0.8, 4, -5.2, 1, -4.2, 1, 1, 4, 4) \tag{23}$$

again gives $(c_1, c_2) = (1, -1)$. The implicit profile (21) is integrated numerically with $U(0) = 0$ and $U'(0) = \sqrt{n/(n+1)}$ for the intensity plot in Figure 2. The numerical integration visualizes an analytically defined smooth orbit; it is not being advertised as a new closed-form Kudryashov solution.

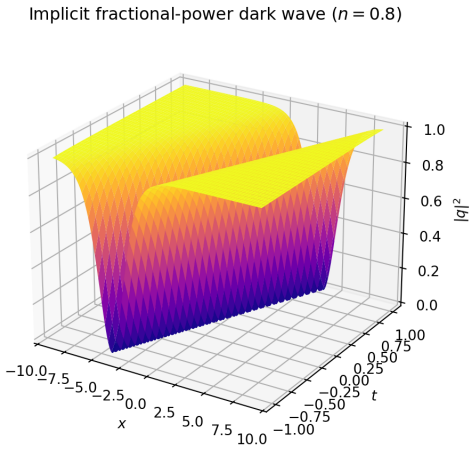



**Figure 2.** Dark-wave intensity $|q(x,t)|^2$ from the implicit heteroclinic orbit for $(n, a, b, \alpha, \beta, \gamma, k, \omega, v) = (0.8, 4, -5.2, 1, -4.2, 1, 1, 4, 4)$.

## 6. Hamiltonian Bifurcation and Equilibrium Classification

A Hamiltonian phase portrait gives a geometric account of why the bright and dark boundary conditions correspond to different wave regimes. The equilibria and their local classifications are determined by the Jacobian of the planar amplitude system, while the conserved energy identifies the homoclinic and heteroclinic trajectories. Correctly computing the Jacobian determinant is essential: reversing its sign interchanges saddle and center classifications and therefore changes the interpretation of the separatrices. Related bifurcation techniques have been employed for other higher-order nonlinear Schrödinger models [19], but the classifications below are derived for the present reduced equation.

With $W = U'$ the amplitude equation becomes

$$U' = W, \qquad W' = -c_1 U - c_2 |U|^{2n} U, \tag{24}$$

with conserved energy

$$H(U, W) = \frac{W^2}{2} + \frac{c_1 U^2}{2} + \frac{c_2 |U|^{2n+2}}{2n+2} = h. \tag{25}$$

The origin $E_0 = (0, 0)$ is always an equilibrium. When $c_1 c_2 < 0$, there are two further equilibria $E_\pm = (\pm U_*, 0)$, with $U_*$ given by (20). The Jacobian is

$$J(U, W) = \begin{pmatrix} 0 & 1 \\ -c_1 - (2n+1) c_2 |U|^{2n} & 0 \end{pmatrix}. \tag{26}$$

Taking the determinant of the *displayed matrix*, rather than inferring its sign from a verbal classification, gives

$$\det J(E_0) = c_1, \qquad \det J(E_\pm) = c_1 + (2n+1) c_2 U_*^{2n} = -2n c_1. \tag{27}$$

Thus, the nontrivial determinant has the opposite sign from the corresponding expression in the earlier submission. Because $\operatorname{tr} J = 0$, a negative determinant gives a saddle and a positive determinant gives purely imaginary linear eigenvalues. Here, the conservative Hamiltonian additionally establishes that the elliptic equilibria are nonlinear centers, rather than unstable foci. For $c_1 < 0, c_2 > 0$, $E_0$ is a saddle and $E_\pm$ are centers; for $c_1 > 0, c_2 < 0$, $E_0$ is a center and $E_\pm$ are saddles. The degenerate case $c_1 = 0$ must be treated separately and is not classified by this linear test.

For the bright choice (19), the zero-energy separatrices form homoclinic loops about the nonzero centers (Figure 3). For the fractional dark choice (23), the energy $H_*$ separatrices connect the two nonzero saddles and are precisely the kink orbit specified by (21) (Figure 4). The topology establishes boundary behavior, not spectral orbital stability of the solitary wave.

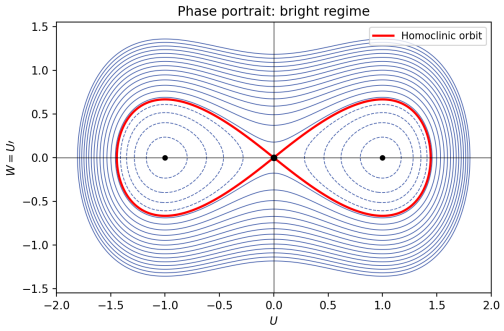



**Figure 3.** Phase portrait for $(n, a, b, \alpha, \beta, \gamma, k, \omega, v) = (0.8, 4, 2, 1, 1, 1, 1, 2, 6)$, giving $c_1 = -1, c_2 = 1$. Red trajectories are homoclinic separatrices.

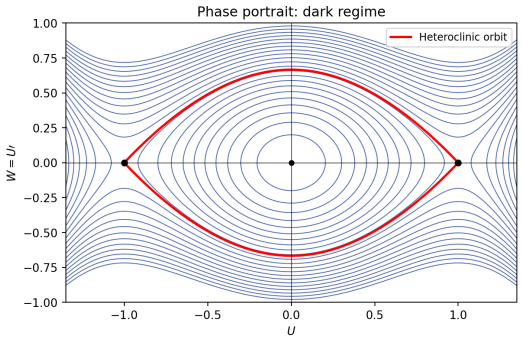



**Figure 4.** Phase portrait for $(n, a, b, \alpha, \beta, \gamma, k, \omega, v) = (0.8, 4, -5.2, 1, -4.2, 1, 1, 4, 4)$, giving $c_1 = 1$, $c_2 = -1$. Red trajectories are heteroclinic separatrices.

## 7. Benjamin–Feir (Modulation) Instability of the Continuous Wave

Traveling-wave existence does not answer whether a spatially uniform carrier state is resistant to small modulations. We therefore perform a separate linear stability calculation for the continuous-wave background, introducing complex sideband perturbations and deriving a dispersion relation from the Fourier coefficient matrix. A nonreal modulation frequency produces exponential growth, and its imaginary part determines the instability band and gain. High-order dispersion is known to influence modulation-instability dynamics in related systems [20]; here, the algebra is evaluated for the specific third-order-dispersive, derivative-nonlinear model, with an explicitly stated gain convention and no implication of solitary-wave spectral stability.

For $A_0 > 0$, the spatially uniform CW is

$$q_0(t) = A_0 e^{ibA_0^{2n}t}. \tag{28}$$

Set $q = (A_0 + \varepsilon)e^{ibA_0^{2n}t}$ and retain terms linear in $\varepsilon$ and $\varepsilon^*$. This gives

$$i\varepsilon_t + a\varepsilon_{xx} + i\alpha\varepsilon_{xxx} + bnA_0^{2n}(\varepsilon + \varepsilon^*) + i(\beta + n\gamma)A_0^{2n}\varepsilon_x + in\gamma A_0^{2n}\varepsilon_x^* = 0. \tag{29}$$

This linearization applies to a CW, so the traveling-wave compatibility constraints (6) need not be imposed for the independent CW spectrum.

To make the determinant calculation explicit, write $\varepsilon = f + ig$, set $S = A_0^{2n}$, and use Fourier amplitudes $(\hat{f}, \hat{g})e^{i(Kx-\Omega t)}$. The real system is

$$\begin{pmatrix} -aK^2 + 2bnS & i(\Omega + \alpha K^3 - \beta SK) \\ -i[\Omega + \alpha K^3 - (\beta + 2n\gamma)SK] & -aK^2 \end{pmatrix} \begin{pmatrix} \hat{f} \\ \hat{g} \end{pmatrix} = 0. \tag{30}$$

Its determinant vanishes precisely when

$$[\Omega + \alpha K^3 - (\beta + n\gamma)SK]^2 = K^2\left[a^2K^2 - 2abnS + n^2\gamma^2S^2\right]. \tag{31}$$

The matrix in this section is the *CW perturbation matrix*, not the phase-plane Jacobian (26); the determinants of both matrices have been explicitly recomputed.

Accordingly,

$$\Omega = -\alpha K^3 + (\beta + n\gamma)SK \pm K\sqrt{a^2K^2 - 2abnS + n^2\gamma^2S^2}. \tag{32}$$

Define $\Delta = 2abnS - n^2\gamma^2S^2$. MI occurs exactly when $\Delta > 0$ and $0 < |K| < K_c$, where

$$K_c = \frac{\sqrt{\Delta}}{|a|}, \qquad g(K) = 2\max\{0, \operatorname{Im}\Omega\} = 2|K|\sqrt{\Delta - a^2K^2} \quad (0 < |K| < K_c). \tag{33}$$

For $a \neq 0$ direct differentiation of $g^2$ gives the corrected optimum and *maximum gain*

$$K_{\max} = \frac{K_c}{\sqrt{2}}, \qquad g_{\max} = \frac{\Delta}{|a|} = |a|K_c^2 = 2|a|K_{\max}^2. \tag{34}$$

The previous expression $g_{\max} = a^2K_{\max}^2$ was incorrect. For fixed $a, b, n, A_0$, larger $|\gamma|$ reduces $\Delta$, whereas $\alpha$ and $\beta$ shift only the *real* modulation frequency of this zero-carrier CW. These statements concern linear CW growth and not nonlinear pulse breakup rates. Figure 5 uses the complete model coefficients $a = 1$, $b = 2$, $\alpha = 1$, $\beta = 1$, $n = 1$, $A_0 = 1$ and the indicated $\gamma$ values; no carrier $k$ or traveling speed $v$ is required for a spatially uniform CW.

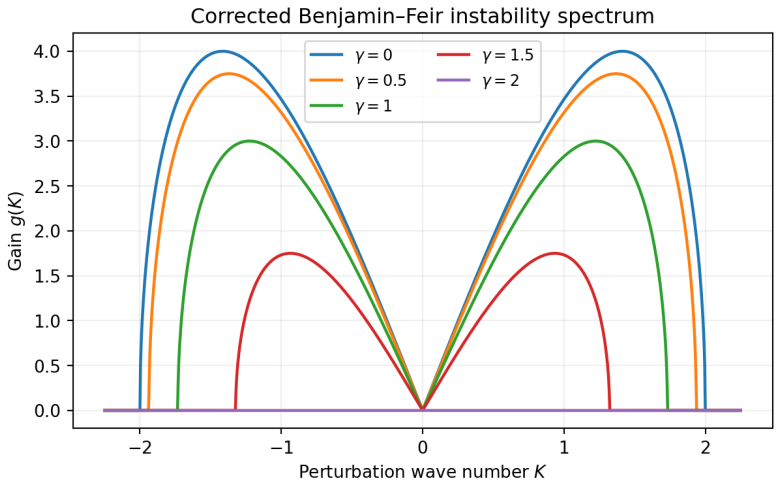



**Figure 5.** CW modulation-instability gain $g(K)$ for $a = 1$, $b = 2$, $\alpha = 1$, $\beta = 1$, $n = 1$, $A_0 = 1$; $\gamma = 0, 0.5, 1, 1.5, 2$ as shown in the legend.

## 8. Conclusions and Scope

The present study examines three distinct aspects of the generalized Schrödinger–Hirota model: the validity of traveling-wave solutions, their consistency with the prescribed asymptotic boundary conditions, and the modulation instability of continuous-wave backgrounds. Direct substitution into the original evolution equation, together with Hamiltonian phase-plane analysis and linear perturbation theory, provides a consistent framework for distinguishing the existence of admissible solitary waves from the stability properties of the continuous-wave state.

The direct substitution analysis demonstrates that the previously proposed free-$b_1$ extended-Kudryashov family and its associated dark-soliton limit do not satisfy the governing equation. However, a special rational solution corresponding to $b_1 = -2$ remains valid as a singular branch restricted to a half-line and therefore does not represent a globally classical optical soliton. For real-valued traveling-wave amplitudes, the reduced equation necessarily involves the nonlinearity $|U|^{2n}U$, with the corresponding Hamiltonian potential $c_2|U|^{2n+2}/(2n+2)$.

Under the derived compatibility conditions, exact bright solitary waves exist for $c_1 < 0$ and $c_2 > 0$, whereas sign-changing dark kinks arise for $c_1 > 0$ and $c_2 < 0$ and can be characterized by an implicit quadrature for arbitrary $n > 0$. For $n > 1/2$, including the fractional-power case $n = 0.8$, these profiles satisfy both components of the original evolution equation classically when the compatibility conditions hold. For $0 < n \leq 1/2$, additional regularity considerations are required at the zeros of the amplitude when $\gamma \neq 0$.

The Hamiltonian bifurcation analysis yields the corrected Jacobian determinant $-2nc_1$ at the nontrivial equilibrium points, establishing the corresponding saddle and center classifications. Furthermore, the Benjamin–Feir instability analysis provides the corrected maximum modulation-instability gain $g_{\max} = \Delta/|a|$ when $\Delta > 0$, under the adopted gain convention. These findings establish the mathematical consistency of the admissible traveling-wave structures and characterize the linear instability of continuous-wave backgrounds. They do not, however, establish the spectral or orbital stability of the localized solitary waves. The identification of additional nontrivial closed-form solution families and the investigation of their spectral stability remain important directions for future research.

**Author Contributions:** Conceptualization, writing—original draft preparation and methodology: O.G.-G.; project administration and supervision: A.B.; software, data curation and investigation: M.H.-S. and A.H.A. All authors have read and agreed to the published version of the manuscript.

**Funding:** This research received no external funding.

**Institutional Review Board Statement:** Not applicable.

**Informed Consent Statement:** Not applicable.

**Data Availability Statement:** All analytical results and numerical illustrations supporting the findings of this study are included in the article.

**Acknowledgments:** The work of the last author (A.B.) was supported by Grambling State University through the Endowed Chair of Mathematics. A.B. gratefully acknowledges this support.

**Conflicts of Interest:** The authors declare no conflicts of interest.

## References

1. Hasegawa, A. Optical soliton: Review of its discovery and applications in ultra-high-speed communications. *Front. Phys.* **2022**, *10*, 1044845. [CrossRef]
2. Maimistov, A.I. Solitons in nonlinear optics. *Quantum Electron.* **2010**, *40*, 756–781. [CrossRef]
3. Hasegawa, A.; Kodama, Y. *Solitons in Optical Communications*; Oxford University Press: Oxford, UK, 1995. [CrossRef]
4. Li, Z.; Li, L.; Tian, H.; Zhou, G. New types of solitary wave solutions for the higher order nonlinear Schrödinger equation. *Phys. Rev. Lett.* **2000**, *84*, 4096–4099. [CrossRef]
5. Hirota, R. Exact envelope-soliton solutions of a nonlinear wave equation. *J. Math. Phys.* **1973**, *14*, 805–809. [CrossRef]
6. Kaur, L.; Arnous, A.H.; Murad, M.A.S.; Biswas, A. Dispersive optical soliton perturbation with Schrödinger–Hirota equation by Lie symmetry. *Ukr. J. Phys. Opt.* **2026**, *27*, 03238–03258. [CrossRef]
7. Uzunov, I.M.; Arabadzhiev, T.N.; Nikolov, S.G. Self-steepening and intrapulse Raman scattering in the presence of nonlinear gain and its saturation. *Optik* **2022**, *271*, 170137. [CrossRef]
8. Uzunov, I.M.; Georgiev, Z.D.; Arabadzhiev, T.N. Influence of intrapulse Raman scattering on stationary pulses in the presence of linear and nonlinear gain as well as spectral filtering. *Phys. Rev. E* **2014**, *90*, 042906. [CrossRef]
9. Chen, B.; Du, S.; Li, D.; Li, B.; Wang, S.; Wang, T. Wavelength conversion process of intra-pulse stimulated Raman scattering in near-zero negative dispersion range. *Photonics* **2025**, *12*, 104. [CrossRef]
10. Biswas, A.; Konar, S. *Introduction to Non-Kerr Law Optical Solitons*; Chapman & Hall/CRC: Boca Raton, FL, USA, 2007.
11. Younas, U.; Hussain, E.; Muhammad, J.; Garayev, M.; El-Meligy, M. Bifurcation analysis, chaotic behavior, sensitivity demonstration and dynamics of fractional solitary waves to nonlinear dynamical system. *Ain Shams Eng. J.* **2025**, *16*, 103242. [CrossRef]
12. Ouahid, L.; Abdou, M.A.; Alshahrani, D.O.; Akgül, A. New periodic wave solution for time-fractional perturbed nonlinear Schrödinger equation arising in optical fiber via newly extended mapping scheme. *Opt. Rev.* **2025**, *32*, 608–618. [CrossRef]
13. Ahmed, K.K.; Ahmed, H.M.; Akgül, A.; Hassani, M.K.; Hendy, A.S.; Samir, I. Identification of stochastic optical solitons in a generalized NLSE characterized by fourth order dispersion and weak nonlocality. *Sci. Rep.* **2025**, *15*, 33805. [CrossRef]
14. Kudryashov, N.A. One method for finding exact solutions of nonlinear differential equations. *Commun. Nonlinear Sci. Numer. Simul.* **2012**, *17*, 2248–2253. [CrossRef]
15. Mahmud, F.; Samsuzzoha, M.; Akbar, M.A. The generalized Kudryashov method to obtain exact traveling wave solutions of the PHI-four equation and the Fisher equation. *Results Phys.* **2017**, *7*, 4296–4302. [CrossRef]
16. Agrawal, G.P. Nonlinear fiber optics: Its history and recent progress [Invited]. *J. Opt. Soc. Am. B* **2011**, *28*, A1–A10. [CrossRef]
17. Kudryashov, N.A. Stationary solitons of the generalized nonlinear Schrödinger equation with nonlinear dispersion and arbitrary refractive index. *Appl. Math. Lett.* **2022**, *128*, 107888. [CrossRef]
18. Zayed, E.M.E.; Saad, B.M.M.; Arnous, A.H.; Yildirim, Y.; Biswas, A.; Moraru, L.; Dragomir, C.M.B. Quiescent solitons in magneto-optic waveguides having Kudryashov's first form of nonlinear self-phase modulation structure. *Ukr. J. Phys. Opt.* **2026**, *27*, 02001–02022. [CrossRef]
19. Ouyang, Q.; Zhang, Z.; Wang, Q.; Ling, W.; Zou, P.; Li, X. Solitary, periodic, kink wave solutions of a perturbed high-order nonlinear Schrödinger equation via bifurcation theory. *Propuls. Power Res.* **2024**, *13*, 433–444. [CrossRef]
20. Runge, A.F.J.; Qiang, Y.L.; Pasarelli, N.; de Sterke, C.M. Modulation instability with high-order dispersion: Fundamental limitations of pattern formation. *Opt. Express* **2024**, *32*, 8603–8613. [CrossRef]

**Disclaimer/Publisher's Note:** The statements, opinions and data contained in all publications are solely those of the individual author(s) and contributor(s) and not of MDPI and/or the editor(s). MDPI and/or the editor(s) disclaim responsibility for any injury to people or property resulting from any ideas, methods, instructions or products referred to in the content.